INORGANIC CHEMISTRY
FRONTIERS

RESEARCH ARTICLE

View Article Online
View Journal

Cite this: DOI: 10.1039/d5qi01976a

A robust and flexible Cu-based metal–organic framework for gas separation and volatile organic compounds detection

Pablo Salcedo-Abraira, *†[a] Víctor K. Abdelkader-Fernández, †[a] María Laynez,[a] Sara Rojas,[a] Alfonso Salinas-Castillo,[b] Manuel Pérez-Mendoza[a] and Antonio Rodríguez-Diéguez *[a]

Received 29th September 2025,
Accepted 28th November 2025

DOI: 10.1039/d5qi01976a

rsc.li/frontiers-inorganic

In the continuous search for new materials able to interact with CO_2 and Volatile Organic Compounds (VOCs), metal–organic frameworks (MOFs) have emerged as an outstanding class in CO_2 adsorption and VOCs detection. Particularly, Cu-based MOFs with coordinatively unsaturated sites (CUS) are considered one of the most appealing class of MOFs due to their ability to interact with these gases. In this work, a novel MOF named GR-MOF-26, based on copper and the combination of the 5-amino-2,4,6-triiodoisophthalic acid (H_2atiip) and 4,4′-bipyridyl (bipy) ligands, is reported. This material presents Cu CUS with a square-planar pyramid geometry and exhibits permanent porosity (specific Dubinin–Radushkevich surface area of 150 $m^2\ g^{-1}$) combined with a strong light absorption in almost the entire UV-Vis spectrum range (with a reflectance maximum at 510 nm), excellent chemical stability in different organic solvents and in a broad range of pH (from 3 to 10), and moderate selectivity for CO_2 adsorption (0.98 mmol g^{-1} at 1 bar and 2.1 mmol g^{-1} at 24 bar) over CH_4. Further, single-crystal X-ray diffraction studies demonstrated that GR-MOF-26 is able to reversibly change its structure and colour upon exposure to different hydrophilic VOCs, and the driving force for these changes is a combination of different parameters (such as pore content, modification of the Cu coordination sphere and/or the structural flexibility).

Introduction

The development of society towards the end of the 20th century and, more importantly, during the last decades, has become associated with technological progress that has improved social welfare in an outstanding way.[1] However, this development has been accompanied by unprecedented environmental contamination.[2] With the increasing greenhouse gas (such as CO_2) emissions, humans are supercharging the natural greenhouse effect, causing global temperature rise. The consequences of climate change now include intense droughts, water shortages, severe fires, rising sea levels, floods, melting of the poles, catastrophic storms and declining biodiversity, among others. Moreover, the presence of emerging organic contaminants (EOCs) from items such as personal care products or pharmaceutical drugs,[3,4] present some of the current problems that need to be solved in order to preserve the planet. In particular, volatile organic compounds (VOCs) are an important class of EOCs that can be found in various products (*i.e.*, glue, upholstered furniture) which have a high vapor pressure at room temperature. VOCs have increased volatility and mobility, and resistance to degradation, being able to be transported over long distances in the environment.[5] Some common VOCs are the aromatic hydrocarbons (*i.e.,* benzene, toluene, xylene and ethyl benzene); halogenated hydrocarbons (*i.e.,* chloroethylene and trichloroethylene); and other organic compounds (*i.e.,* dichloromethane, acetone and isopropyl alcohol). Some VOCs are toxic to humans or cause harm to the environment. Further, exposure to VOCs that are not acutely toxic can lead to long-term health effects. The VOC Solvents Emissions Directive 1999/13/EC from the European Union required the installation of measures to reduce the industrial emissions of VOCs for activities where solvents are used (*i.e.*, printing, surface cleaning, manufacture of footwear and pharmaceutical products) and according to certain values (*i.e.*, total emission limit of 5% of solvent input when manufacturing pharmaceutical products).[6] Therefore, it is necessary to determine the presence and indoor concentrations of VOCs.

Metal–organic frameworks (MOFs) are hybrid polymeric materials based on inorganic units linked by polytopic organic

[a]*Department of Inorganic Chemistry, University of Granada, Av. Fuente nueva s/n, 18071 Granada, Spain. E-mail: psalcedo@ugr.es, antonio5@ugr.es*
[b]*Department of Analytic Chemistry, University of Granada, Av. Fuente nueva s/n, 18071 Granada, Spain*
† Equally contributing authors.

ligands that exhibit outstanding porosity (up to 7000 $m^2\ g^{-1}$), with a large variety of crystalline structures and an easily tuneable chemical composition.[7–10] In the last decades, MOFs have attracted growing attention due to their versatility and potential application in different relevant fields (*e.g.*, capture and separation of fluids, energy generation, catalysis, biomedicine).[11] Regarding gas–MOF interactions, MOFs with coordinatively unsaturated sites (CUS) and organic ligands containing free amino groups have typically exhibited good performance for CO_2 capture due to CO_2 chemisorption on the CUS that act as Lewis acid sites,[12–15] and the CO_2 affinity for amino groups.[16] MOFs have been also used as sensors for VOCs due to their host–guest interactions triggering different and specific responses (from changes in their optical properties to their electronic and mechanical properties).[17,18] Particularly, Cu-based MOFs present a large variety of secondary building units (SBUs, forming atomic Cu in different coordination geometries such as octahedra, square-based pyramid or square planar to more complex clusters such as paddlewheel)[19,20] due to the particular electronic configuration of Cu^{2+} compared with other first-row transition metal cations, as a consequence of the Jahn–Teller effect.[21] In addition, the preparation of Cu-based MOFs has been of great interest, yielding very interesting results for CO_2 separation.[22] Thus, the preparation of Cu-based MOFs with accessible CUS with interesting properties is made relatively easy by using Cu as a metallic node.[23] In addition, halogen-containing ligands have demonstrated good potential in the development of materials for CO_2 separation, due to the potential interaction of CO_2 with the halogen atoms.[24]

Here, we report a new material, named GR-MOF-26, based on copper and the combination of the 5-amino-2,4,6-triiodoisophthalic acid (H_2atiip) and 4,4′-bipyridyl (bipy) ligands. GR-MOF-26, or $[Cu(atiip)(bipy)(H_2O)]\cdot 5H_2O$, exhibits a flexible porous 3D structure with accessible CUS and free NH_2 groups. This material presented a moderate selectivity for CO_2 adsorption over CH_4. The potential interactions of the CO_2 molecule were evaluated by using the isostructural CS_2 molecule and single-crystal X-ray diffraction (SC-XRD). Additionally, GR-MOF-26 exhibits a reversible change in its structure and colour upon exposure to different VOCs, which reinforces its potential in the development of VOCs detectors.

Results and discussion

Synthesis and physicochemical characterization

A novel material, branded GR-MOF-26 (from University of Granada MOF), was prepared by a simple reaction under aqueous conditions (see experimental section for further details). The material, based on Cu and the 5-amino-1,3,6-triiodoisophthalic acid (H_2atiip) and 4,4′-bipyridyl (bipy) ligands, crystallizes on the monoclinic system with the *Cc* space group (Table S1), with unit cell parameters of a = 12.4308 Å, b = 18.3450 Å, c = 11.9896 Å, β = 102.470°, and with a V = 2669.6 $Å^3$. The structure, elucidated by single crystal X-ray diffraction (SC-XRD), is built up from CuO_3N_2 square-base pyramids as SBUs that are linked by the atiip and bipy ligands, resulting in a 3D network (Fig. 1). The coordination sphere of the Cu atoms is constituted by two nitrogen atoms from different bipy ligands located in the basal plane in opposite positions, two oxygen atoms from the carboxylate groups of the atiip ligands acting as monodentate in the other two basal positions, and finally, one oxygen from a water molecule in the apical position of the pyramid (Fig. S1 and Table S2). The bipy coordination to the Cu centres leads to Cu-bipy-Cu chains in two different directions (with a torsion angle between them of 86.08°) that are bonded by the atiip ligand in a *cis* conformation, generating the 3D network. This network presents voids (9 × 8.5 × 6.5 $Å^3$) where water molecules are located (representing 22% of the unit cell volume), creating H-bonds among the carboxylate groups of the atiip ligands, the coordinated water molecules and themselves (Fig. S2).

The purity of the polycrystalline sample was evaluated by powder X-ray diffraction (PXRD). Pawley profile fitting showed no significant differences in the unit cell parameters (Fig. S3 and Table S3) evidencing the absence of crystalline impurities, in good agreement with elemental analysis of light elements (theo. % C 24.9, N 4.84, H 2.32; exp. % C 24.57 ± 0.07, N 4.71 ± 0.06, H 2.33 ± 0.04).

Fourier transformed infrared spectroscopy (FTIR, Fig. S4) also confirmed the coordination of the ligands to the metal centre, as observed by the shift of the bands of the carboxylate groups (from 1702 and 1661 cm^{-1} to 1592 cm^{-1}). The material also presented a shift on the νN–H bands coming from the atiip amino group (from 3360 and 3452 cm^{-1} to 3348 and 3403 cm^{-1}) and a broad band at around 3600 cm^{-1} corresponding to the νO–H from water molecules.

The thermal stability was evaluated by thermogravimetric analysis (TGA, Fig. S5) and variable-temperature powder X-ray diffraction (VT-PXRD, Fig. S6). The TGA curve showed a first weight loss from room temperature (RT) to 150 °C of *ca.* 10%, which fits with 4.9 water molecules, in relatively good agreement with crystallographic data (5 molecules in TG *vs.* 6 in SC-XRD). Note here that this small difference may come from the hydration state of the material, which could get slightly dried with time. Finally, the material decomposes at around 250 °C, yielding CuO as the final residue of the combustion and confirming the purity of the material (theo. final residue based on dried material 10.24%; exp. final residue 10.05%). VT-PXRD showed a progressive structure transformation upon heating (from 30 to 60 °C), mostly due to the network flexibility from the loss of water molecules. Then, the structure remains stable (from 60 to 210 °C) before its amorphization at temperatures above 210 °C, in agreement with TGA data.

Furthermore, the chemical stability of GR-MOF-26 in different media (organic solvents, aqueous solutions at different pH) was evaluated by putting the solid in suspension (2 mg mL^{-1}) and leaving it under stirring overnight (see experimental section for further details). After recovery of the solids in organic solvents, a colour change of the samples was observed (Fig. S7), and the original colour was recovered after drying the solids under air. PXRD patterns of the dried solids

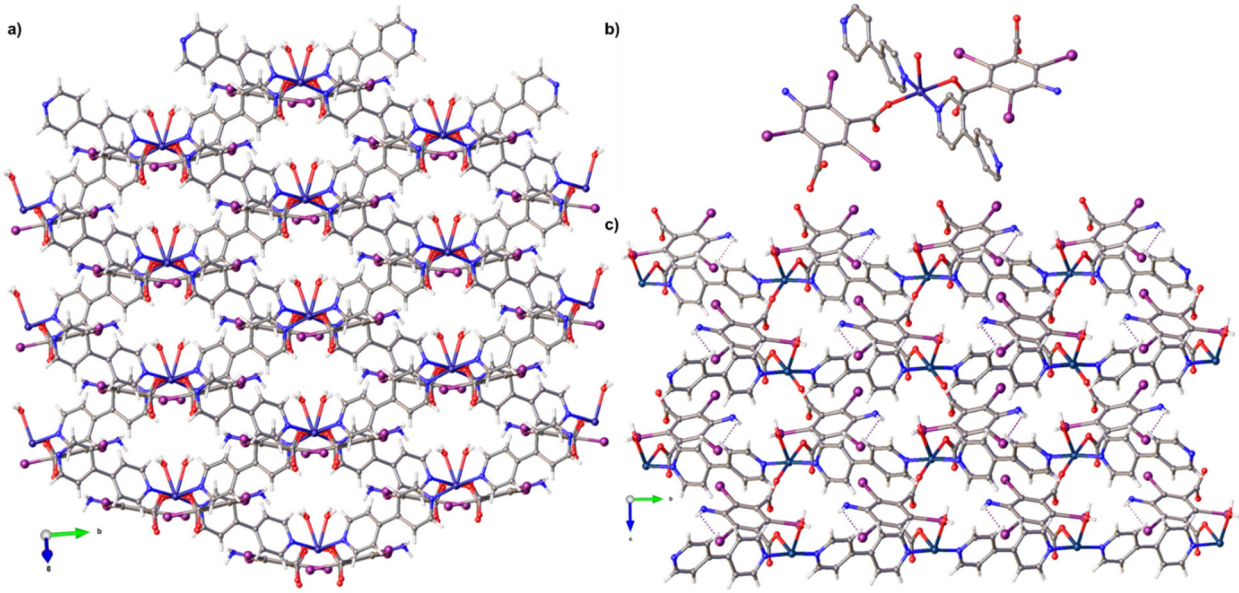

Fig. 1 (a) GR-MOF-26 crystalline structure view along the pore channels, (b) SBU of the GR-MOF-26 and (c) view along the *a* axis. Copper, iodine, oxygen, nitrogen, carbon and hydrogen are represented by electric blue, purple, red, blue, grey and white, respectively. Free water molecules were removed for clarity.

revealed that the crystalline structure of GR-MOF-26 was maintained in all cases, evidencing the material robustness in these media (Fig. S8). On the one hand, in aqueous solutions, PXRD revealed that the crystalline structure was maintained in a broad range of pH ($3 < pH < 10.5$), being only slightly altered by the appearance of two new peaks at *ca.* 12 and 19° at all pH values, with the exception of water (pH = 5.4, Fig. S9). These structural changes might be related to network flexibility (as these peaks also appear in VT-PXRD during the phase transformation), but possible structural changes due to some protonation or deprotonation of the water molecule of the SBU, the interaction of the added counterions (*i.e.* Na^+ for the alkali and Cl^- for the acidic conditions) or the addition of an extra molecule to the Cu coordination sphere cannot be discarded, or even a combination of these effects. On the other hand, samples at pH 1.5 and 12.1 (Fig. S9) presented completely different PXRD patterns, indicating the instability of the material in these conditions. Additionally, the ligand released during the experiments was quantified by HPLC (Table S4 and Fig. S10). It was observed that GR-MOF-26 presented almost no degradation (0.5% bipy and 2% atiip release) at pH between 5.4 and 8.2, being slightly degraded at pH 3 (1.7% bipy and 6.6% atiip) and 10.5 (4% bipy and 17.5% atiip) and completely degraded at pH 12. Note here that the absence of ligand release at pH 1.5 is due to ligand precipitation upon MOF degradation. The stability in aqueous media of GR-MOF-26 is much higher than usual for Cu(II)-based carboxylate MOFs[25] (and others such as phosphonate-based MOFs),[19] which are typically not stable and tend to easily degrade and/or dissolve upon contact with water. The robustness of GR-MOF-26 might be a consequence of the presence of a N-donor co-ligand in the structure combined with the presence of CUS where the water molecules could interact, avoiding the hydrolysis of the Cu-ligand bonds.

Finally, the optoelectronic properties of GR-MOF-26 were evaluated by UV-Vis spectroscopy. Diffuse reflectance and absorbance spectra (Fig. S11) showed that GR-MOF-26 presents strong light absorption in the entire range (200–800 nm), with a slightly lower absorption around 510 nm, leading to the characteristic green colour of GR-MOF-26.

Gas sorption properties

The textural properties of the solid were evaluated by N_2 sorption isotherms. Considering both the crystallographic voids and the relatively easy removal of water molecules, some N_2 uptake was expected; however, the adsorbed N_2 amount was almost negligible (Fig. S12). Moreover, low-pressure CO_2 sorption experiments at 273 K (Fig. 2) evidenced the porosity of GR-MOF-26, presenting a type-I isotherm with a specific surface area of 150 $m^2\ g^{-1}$ and pore volume of 6×10^{-2} $cm^3\ g^{-1}$ (calculated with the Dubinin–Radushkevich equation[26]) and adsorbing up to 0.98 mmol g^{-1} (*i.e.* 0.78 molecules of CO_2 per unit formula) at 1 bar.

Furthermore, high-pressure experiments were carried out to study the CO_2 selectivity of GR-MOF-26 over other gases. In particular, CO_2 and CH_4 isotherms were collected at 273 K. Fig. 3 clearly shows almost no adsorption of CH_4 in the entire range; meanwhile, for CO_2, type-I and III isotherms (type I at the beginning, in agreement with the low-pressure data, and type III at high pressure) are observed, evidencing the selectivity of CO_2 over CH_4 and the potential capacity of the GR-MOF-26 as CO_2 adsorbent.

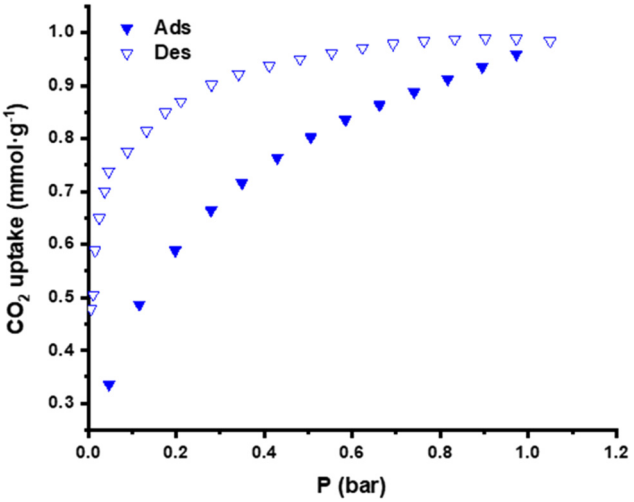

Fig. 2 Low-pressure CO_2 sorption isotherm at 273 K of GR-MOF-26.

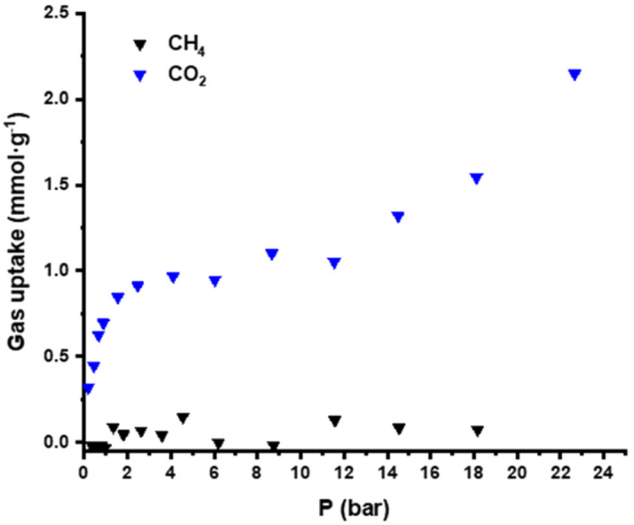

Fig. 3 High-pressure CO_2 and CH_4 sorption isotherms at 273 K of GR-MOF-26.

Additionally, the CO_2 isotherm presented a second adsorption region at high pressures (from 12 to 24 bar), reaching up to 2.1 mmol g^{-1} (*i.e.* 1.66 CO_2 molecules per unit formula). As the adsorption process occurs in two steps, one could hypothesize that the first one might be attributed to chemisorption, and meanwhile, the second one could correspond to the molecules adsorbed in the pores. The modest adsorption values at low pressure exhibited by GR-MOF-26 are in line with those reported in the literature for well-known materials such as MIL-101(Cr), SNU-70 or MOF-177, among others (with 1.17, 0.80 and 0.77 mmol g^{-1} at 1 bar and 298 K, respectively, see Table S5).[27] However, the values are lower than that obtained with some halogen-decorated porous MOFs (around 2 mmol g^{-1})[24] and far from other Cu-based MOFs (such as the well-known HKUST-1, with 4.16 mmol g^{-1} at 1 bar and 298 K) or some of the highest reported ones (such as Mg-MOF-74 with 8 mmol g^{-1} at 1 bar and 296 K).[27]

In order to shed some light on the potential CO_2 interactions with the framework, and due to the similar molecular shape and electronic properties between molecules, activated crystals of GR-MOF-26 were immersed in CS_2 (see experimental section for further details) and then studied by SC-XRD (Table S6). Note here that despite the weaker electrophile properties and the tendency to form chalcogen bonds, CS_2 can be used to crystallographically estimate the location of CO_2 gas molecules inside the pores.[28,29] After exposure of GR-MOF-26 to CS_2, the diffraction experiments showed a significant change in the structure (Table S6 and Fig. S13), from a *Cc* to $P2_1/c$ space group. The *a* and *b* lattice parameters were mostly unaltered, being only *c* and β modified (from 11.9896 to 10.844 Å for *c* and from 102.47 to 104.47° for β), resulting in a reduction in cell volume compared with the pristine GR-MOF-26 (from 2669.6 to 2405 $Å^3$). The SBU was also modified, being the carboxylate groups in *trans* conformation with respect to the Cu (Fig. S14). Also, the coordinated water molecule placed on top of the pyramid is removed, leading to the formation of a square-planar geometry. Furthermore, two water molecules were located close to the Cu atoms but not coordinating them (*d*Cu···Ow 2.72 Å). These changes in structure also led to a pore size reduction when compared with the pristine material (from 9 × 8.5 × 6.5 $Å^3$ to 8 × 7.5 × 6 $Å^3$, and from 22 to 17% of the U.C.). Finally, half CS_2 molecule per unit formula was found, being in the pockets of the structure and mainly interacting with the aromatic ring of the atiip carboxylate linker (*d*S···aromatic ring atiip 3.46 Å) through a chalcogen bond (Fig. S15). Interestingly, the voids where the CS_2 molecules are located were aligned in one direction, with the molecules twisted 45° between them (Fig. S13). The rows of pockets were separated from each other in the perpendicular plane, creating a chessboard motif.

The slight difference between the amount of CO_2 molecules quantified by gas sorption and the CS_2 found by diffraction (0.78 *vs.* 0.5 molecules per unit formula of GR-MOF-26) could be rationalized as follows: (i) the larger size of CS_2 compared with CO_2; (ii) different polarity of the molecules, the CS_2 being capable of establishing chalcogen bonds; and (iii) the presence of water molecules in the structure close to the Cu atoms that hinder the potential chemisorption of CS_2. Despite these differences, the values reached at low pressure for CO_2 were very close to those obtained crystallographically for CS_2, so it could be considered that the CO_2 molecules were potentially located at similar positions compared to CS_2. Despite the initial hypothesis that led to the ligand selection, the NH_2 group seems to not interact with the CO_2 or CS_2 molecules. This is probably due to the steric hindrance of the bulky iodine atoms of the ligand, and the H-bonding interaction between the amino group and one of the iodine atoms of the same ligand (as can be observed in Fig. 1c).

Exposure to volatile organic compounds

Due to the CO_2 and CS_2 sorption capability demonstrated by GR-MOF-26 and its structure flexibility, this material was eval-

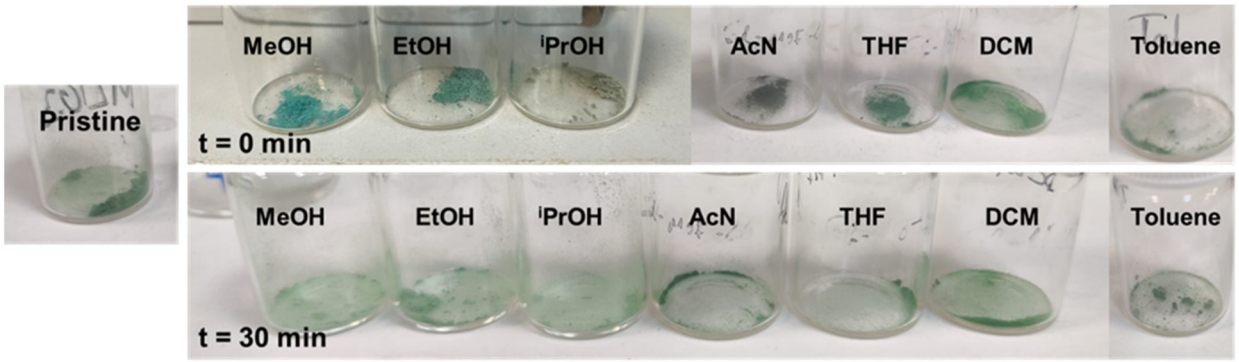

Fig. 4 Change of colour of GR-MOF-26 after 24 h of exposure to different organic vapours (t = 0 min, top) and after 30 min of exposition to air (t = 30 min, bottom).

uated for the capture of different VOCs, including methanol (MeOH), ethanol (EtOH), isopropanol (^{i}PrOH), acetonitrile (AcN), tetrahydrofuran (THF), dichloromethane (DCM) and toluene. The solid was put in contact with a saturated atmosphere of each VOC for 24 h and then evaluated by SC-XRD (Tables S7–S11). Note here that prior to the SC-XRD analyses, a change in colour of the material was observed (Fig. 4, t = 0 min and Fig. S16), indicating a potential change of the structure.

Diffraction experiments showed different results for each of the selected molecules. The exposure to MeOH resulted in a change of the space group from *Cc* to $P2_1/n$, with some changes in the a, c and β parameters and with a small variation in the unit cell volume (see Table 1). These changes were promoted by a change of the SBU, being the carboxylate groups in a *trans* conformation (as in the case of the CS_2) maintaining the coordinated water molecule (Fig. S17). Also, a solvent exchange of the molecules inside the pores occurred, with MeOH molecules instead of water creating the H-bond network in the pores (Fig. S18). These changes resulted in a modification of the pore size (from 9 × 8.5 × 6.5 Å^3 to 9 × 7 × 5 Å^3, from 22 to 20% of the U.C.). In the case of EtOH, the space group changed to $P2_1/c$, with changes in all the unit cell parameters (Table 1). The SBU was modified as in the case of CS_2, presenting a square planar geometry with a *trans* conformation (Fig. S17), and both EtOH and water molecules were found inside the voids (changing to 8.5 × 6.5 × 5.5 Å^3). On the other hand, for ^{i}PrOH, the $P\bar{1}$ space group was found with significant changes in the lattice parameters and the unit cell volume (Table 1).

Here, and as in the case of the MeOH, the coordination of the atiip ligands to the Cu in the SBU changed from *cis* to *trans* conformation, maintaining the coordinated water molecule and, thus, the square-based pyramid geometry. However, no ^{i}PrOH molecules were found inside the pores (that changed from 9 × 8.5 × 6.5 Å^3 to 6.5 × 6 × 4.5 Å^3, from 22 to 11% of the U.C.), probably due to the larger size of isopropanol compared with the other alcohols, with only water molecules inside. In the case of AcN, the *Cc* space group was maintained with small changes in the lattice parameters compared with the other solvents (Table 1). Regarding the SBU, a change in conformation from *cis* to *trans* was also observed, and the coordinated water molecule was removed, as in the case of EtOH, leading to a square-planar coordination geometry (Fig. S17). Regarding the pore content, exposure to AcN induced the drying of the material, removing not only the coordinated water molecule but also the water molecules inside the pores, causing a reduction in the unit cell volume and in the pore size (from 2669 to 2407 Å^3 and from 9 × 8.5 × 6.5 Å^3 to 6.5 × 5 × 4 Å^3; from 22 to 10% of the U.C. volume). For THF, the space group changed as for the MeOH, from *Cc* to $P2_1/c$, with considerable changes in the unit cell parameters (Table 1). Despite these changes, the SBU remained unaltered compared with the pristine one, with square-based pyramid geometry with the atiip

Table 1 Comparison of the U.C. parameters of GR-MOF-26 structure exposed to different VOCs

Material	Pristine	CS_2	MeOH	EtOH	^{i}PrOH	AcN	THF
Crystal system	Monoclinic	Monoclinic	Monoclinic	Monoclinic	Triclinic	Monoclinic	Monoclinic
Space group	*Cc*	$P2_1/c$	$P2_1/n$	$P2_1/c$	$P\bar{1}$	*Cc*	$P2_1/c$
a/Å	12.4308(6)	12.687(9)	11.618(5)	12.7531(19)	10.336(4)	13.051(3)	14.408(3)
b/Å	18.3450(7)	18.051(2)	18.661(5)	17.863(3)	11.046(3)	17.718(4)	18.410(3)
c/Å	11.9896(5)	10.844(16)	12.499(6)	10.7630(17)	21.105(7)	10.745(3)	18.809(3)
α/°	90	90	90	90	79.03(3)	90	90
β/°	102.470(2)	104.47(16)	106.00(5)	104.340(5)	76.17(3)	104.288(7)	94.124(1)
γ/°	90	90	90	90	82.67(3)	90	90
Volume/Å^3	2669.6(2)	2405(4)	2604.8(2)	2375.5(6)	2288.5(1)	2407.8(1)	4976.3(1)
Z	4	4	4	4	4	4	8
V/Z/Å^3	667.4	601.25	651.2	593.9	572	601.75	622.04

ligands in *cis* conformation (Fig. S17). On the other hand, the pore size decreased (from 9 × 8.5 × 6.5 $Å^3$ to 8 × 5 × 5 $Å^3$, from 22 to 15% of U.C.), presenting only 3.5 H_2O molecules per unit formula instead of the 6 that are present in the pristine GR-MOF-26. Finally, exposure to DCM and toluene does not affect the crystalline structure of GR-MOF-26, as could be expected due to the absence of colour change in the solid. This selective colour change may be rationalized considering the nature of the solvents. Hydrophilic (*i.e.* water miscible) solvents act as desiccator agents to the structure, removing the water molecules (and replacing them in the case of MeOH and EtOH) partially or totally from the pores, and even from the metallic centre. These three phenomena, individually or in combination, appear to be the driving force of the colour change. On the other hand, hydrophobic (*i.e.* non-water-miscible) solvents did not affect the structure, as they cannot be mixed with water, thus hindering the drying of the framework. Very interestingly, when the material is re-exposed to the atmosphere in the absence of hydrophilic organic solvents, the pristine colour (and potentially the original structure) is recovered (Fig. 4, t = 30 min and Fig. S16).

The structural change reversibility was confirmed by PXRD of the samples at t = 30 min (Fig. S19–S23), which presented a similar diagram to that of the pristine material. In order to corroborate the transformation in the bulk materials, TGA experiments were performed in the freshly exposed samples with the guest molecules inside the pores (*i.e.* MeOH, EtOH, ^{i}PrOH and THF, Fig. S24). The curves showed initial weight losses in good agreement with the expected guest molecules. The sample exposed to MeOH exhibited a two-step weight loss of a 12.8% (corresponding to 2.2 MeOH molecules and 1 coordinated H_2O molecule) with a clear change in the slope, corresponding to an initial departure of the MeOH molecules followed by the removal of the coordinated water molecule. For EtOH, the loss is progressive (6%, 1 water molecule and 0.5 EtOH) up to 230 °C, probably due to strong interaction between the solvent and the water molecules inside the pores. On the other hand, both ^{i}PrOH and THF retain the same curve shape as the pristine material but with different initial losses (6.4 and 9.2%, respectively), as consequence of the different amount of water molecules inside each structure (2 and 3.5, respectively).

This reversibility and change of colour depending on the studied VOCs could allow the building of specific sensors for different hydrophilic organic molecules (MeOH, EtOH, ^{i}PrOH, AcN and THF). To further understand these colour changes, diffuse reflectance UV-Vis of the freshly exposed samples was carried out (Fig. S25). In all cases, a hypsochromic shift and/or the appearance of additional reflection bands can be clearly observed (Table S12). The bands of the MeOH, EtOH and AcN samples were shifted to 489, 499 and 495, respectively, while ^{i}PrOH presented a shift to 499 nm and an additional small shoulder at 400 nm; and finally, the THF sample only presented an additional shoulder at 400 nm, remaining the main band at 510 nm with no changes. A rationalization of these phenomena in relation with the structural changes was attempted; however, there is no correlation between them, indicating that the modification of the properties is due to a combination of diverse parameters (coordinated water to the metal centre, coordination conformation of the ligands, pore content). In addition, UV-Vis spectra of the heated sample at 95 °C (*i.e.* after the phase transition) was also collected (Fig. S26). Here, a shift in the band was observed from 510 to 502 nm, with the appearance of a shoulder at 400 nm as in the case of samples exposed to ^{i}PrOH and THF. As at this temperature, there are no water molecules inside the pores (according to TGA), the role of pore content on the colour change mechanism was confirmed. One simple but very important parameter here that is worth highlighting is the fact that all these interactions with VOC molecules (from their absorption to the change of the GR-MOF-26 colour) occurred without a previous drying (with or without vacuum) step, which means that the material could be used as a sensor, without the need for any maintenance or regeneration operation. It worth highlighting here that a device based on Arduino® that is able to detect and differentiate between the hydrophilic VOCs is currently under development in our lab.

Experimental section

Synthesis of GR-MOF-26 {$[Cu(C_8H_2O_4NI_3)(C_{10}H_8N_2)(H_2O)]\cdot 5H_2O\}_n$ or {$[Cu(atiip)(bipy)(H_2O)]\cdot 5H_2O\}_n$ (MW = 884.62 g mol^{-1})

In a 20 mL glass vial, 11.9 mg of $Cu(NO_3)_2\cdot 3H_2O$ (0.05 mmol) was dissolved in 5 mL of distilled water. Then, 5 mL of a previously prepared aqueous solution containing 11.2 mg of 5-amino-1,3,6-triiodoisophthalic acid ($C_8H_2O_4NI_3$ or H_2atiip, 0.02 mmol) and 3.9 mg of 4,4′-bipyridyl ($C_{10}H_8N_2$ or bipy, 0.025 mmol) were added. The obtained green solution was heated at 95 °C for 72 h. After cooling to room temperature, the resulting green crystals were filtered and washed with water (yield = 60%).

Scaled-up synthesis

In a 125 mL glass jar, 119 mg of $Cu(NO_3)_2\cdot 3H_2O$ (0.5 mmol) was dissolved in 25 mL of distilled water. Then, 25 mL of a previously prepared aqueous solution containing 112 mg of 5-amino-1,3,6-triiodoisophthalic acid (H_2atiip, 0.2 mmol) and 39 mg of 4,4′-bipyridyl (bipy, 0.25 mmol) were added. The obtained green solution was heated at 95 °C for 72 h. After cooling to room temperature, the resulting green solid was filtered and washed with water (yield = 60%).

CS_2 adsorption experiments

GR-MOF-26 crystals were heated in an oven at 150 °C for 2 h. Then, the sample was recovered and immediately poured on carbon disulfide and let sit for 24 h. After that, the crystals were immediately analysed by SC-XRD.

Adsorption of VOCs

First, 12 mg of GR-MOF-26 was placed inside an open glass vial. Then, the vial was introduced into a closed container with a saturated atmosphere of different VOCs, including methanol (MeOH), ethanol (EtOH), isopropanol (^{i}PrOH), acetonitrile (AcN), tetrahydrofuran (THF), dichloromethane (DCM) and toluene, for 24 h. After the exposure, the crystals were recovered and immediately analysed by SC-XRD.

Crystallographic studies

Single-crystal X-ray diffraction experiments were performed on a Bruker D8 Venture diffractometer equipped with Mo Kα radiation (0.71073 Å) at room temperature for GR-MOF-26 and at 150 K for the gas exposed samples. Suitable single crystals were mounted on MiTeGen polymer loop using FOMBLING oil. The data reduction was performed with the APEX3 software, and absorption correction was performed using SADABS for GR-MOF-26, GR-MOF-26_EtOH and GR-MOF-26_AcN; and with the CrysAlisPro software and applying the ABSPACK absorption correction for GR-MOF-26_CS2, GR-MOF-26_MeOH, GR-MOF-26_iPrOH and GR-MOF-26_THF. GR-MOF-26_iPrOH crystal was found to be twinned, and thus, processed as two-component twin. The crystalline structures were solved and refined using the SHELX software package[30,31] and Olex2 software.[32] All non-H atoms were refined anisotropically when the resolution data allowed it. H atoms were placed in calculated positions and refined with idealized geometries. Crystallographic data (excluding structure factors) have been deposited with the Cambridge Crystallographic Data Centre as a supplementary publication (CCDC 2402172–2402178).

Physicochemical characterization

Routine powder X-ray diffraction (PXRD) data were collected on a BRUKER D8 DISCOVER equipped with microfocus CuKα radiation (λ = 1.54059 Å) in a 2θ rage of 4–50° with a 2° step size and 40 s of acquisition time. Variable temperature powder X-ray diffraction experiments were performed on a Bruker D8 DISCOVER equipped with monochromated CuKα_1 radiation, 2 mm anti-scatter slits, 2.5° Soller slits and a EIGER detector. Each diffractogram was collected from 5 to 55° (2θ) over 60 min. The sample was heated in an HTK1200N heating chamber from Anton Paar with a 10 °C min^{-1} heating ramp and with a dwell time of 300 s before the data acquisition. Fourier transformed infrared (FTIR) spectra were collected on a BRUKER TENSOR 27FT-IR spectrophotometer in the attenuated total reflectance (ATR) mode. Thermogravimetric analyses (TGA) were performed on a Shimadzu TGA-50H equipment. Ultraviolet–visible (UV-Vis) spectroscopic experiments were performed with a CARY-5E UV-Vis-NIR VARIAN spectrophotometer equipped with a praying mantis accessory. Ligand release quantification was performed by employing a high-performance liquid chromatography (HPLC) equipment (Shimadzu) with an SPD-M40 photodiode array (PDA) UV-Vis detector and a SIL-40C autosampler employing a Shim-pack GIS reverse-phase column (4 μm, 4.6 × 150 mm) at 40° C.

Standard gas adsorption measurements (up to atmospheric pressure) were conducted using a commercial surface area and porosity analyser (ASAP 2020, Micromeritics® Instrument Corporation, GA, US). The N_2 adsorption–desorption isotherms were obtained at 77 K, while CO_2 isotherms were recorded at 273 K. Additionally, the CH_4 and CO_2 capture capacity of GR-MOF-26 under high pressure (up to *ca.* 24 bar) was studied by acquiring the corresponding adsorption isotherms using a custom-built volumetric adsorption apparatus —equipped with stainless steel gas lines and valves to ensure leak-free operation at high pressures. Adsorption of both gases was examined at a temperature of 273 K. Both low-pressure and high-pressure adsorption experiments were preceded by activation/degasification of the GR-MOF-26 sample by applying vacuum and heating at 90 °C for 12 hours. Furthermore, after each adsorption measurement, free-space volume determinations were performed using He gas.

Conclusions

A novel material named GR-MOF-26, which is based on Cu, bipy and atiip, has been successfully synthesized. This solid exhibits a porous flexible structure combined with coordinatively unsaturated sites (CUS) coming from the square-based pyramid coordination geometry of the Cu atoms, a strong UV-Vis absorption in almost the entire UV-Vis spectrum, combined with excellent chemical stability in different organic solvents and in aqueous solution at different pH (3 < pH < 10.5). GR-MOF-26 was also capable of adsorbing up to 0.78 CO_2 molecules per unit formula at 1 bar and 1.25 molecules at 24 bar; no adsorption for CH_4 molecules was observed. Due to the similar shape and isoelectronic structure with CO_2, CS_2 was used to evaluate the potential interactions with the framework by SC-XRD. Finally, GR-MOF-26 was exposed to different VOCs, presenting a reversible change in the structure and the colour of the material. The combination of GR-MOF-26 stability, structural flexibility and selectivity for different molecules may open the gates to the potential development of efficient devices based on MOFs for gas separation and/or VOC detection.

Author contributions

The manuscript was written through the contributions of all authors. All authors have given approval to the final version of the manuscript. P. S.-A.: investigation, data curation, writing – original draft, supervision, conceptualization, funding acquisition; V. K. and A.-F.: investigation, formal analysis, writing-original draft; M. L.: investigation; S. R.: writing – review and editing, funding acquisition; A. S.-C.: writing – review and editing, funding acquisition; M. P.-M.: writing – review and editing, funding acquisition; A. R.-D.: conceptualization, writing – review and editing, funding acquisition.

Conflicts of interest

There are no conflicts to declare.

Data availability

The data supporting this article (single-crystal crystallographic data of all compounds, PXRD, FTIR, TGA, N_2 sorption isotherm, UV-Vis spectroscopy and variable-temperature PXRD data) have been included as part of the supplementary information (SI). Supplementary information is available. See DOI: https://doi.org/10.1039/d5qi01976a.

CCDC 2402172–2402178 contain the supplementary crystallographic data for this paper.[33a–g]

Acknowledgements

The researchers of this paper want to dedicate this work to all those affected by the isolated depression occurring at high altitude/troposphere levels (DANA in Spanish – Depresión Aislada en Niveles Altos) that occurred in Valencia the 29–30th of October 2024.

This research publication is a part of the projects MOFCycle CNS2022-135779 and Napolion PID2022-139956OB-I00 funded by MCIN/AEI/10.13039/501100011033; FQM-394, ProyExcel_00105, P21_00386 and PLSQ_0018 funded by Junta de Andalucía and TransformMOFs (PPJIA2024-18) funded by Universidad de Granda. S. R. is grateful for the grant (RYC2021-032522-I) funded by MCIN/AEI/10.13039/501100011033 and for El FSE invierte en tu futuro. P. S.-A. thanks Grant JDC2022-048964-I funded by MICIU/AEI/10.13039/501100011033 and by the European Union NextGenerationEU/PRTR. Víctor K. Abdelkader-Fernández was supported by the EMERGIA research project (EMEC_2023_00163, Plan Andaluz, D. 54/1989) funded by the Consejería de Universidad, Investigación e Innovación, Junta de Andalucía. Funding for open access charge: Universidad de Granada.

References

1 E. N. Anderson, The Invention of Science: A New History of the Scientific Revolution. By David Wootton. 2015. Harper Collins, New York. 784 pp., *Ethnobiol. Lett.*, 2016, **7**, 55–58.
2 P. O. Ukaogo, U. Ewuzie and C. V. Onwuka, *Microorganisms for Sustainable Environment and Health*, Elsevier, 2020, pp. 419–429.
3 S. Haddad, I. Abánades Lázaro, M. Fantham, A. Mishra, J. Silvestre-Albero, J. W. M. Osterrieth, G. S. Kaminski Schierle, C. F. Kaminski, R. S. Forgan and D. Fairen-Jimenez, Design of a Functionalized Metal–Organic Framework System for Enhanced Targeted Delivery to Mitochondria, *J. Am. Chem. Soc.*, 2020, **142**, 6661–6674.
4 E. Antunes, A. K. Vuppaladadiyam, A. K. Sarmah, S. S. V. Varsha, K. K. Pant, B. Tiwari and A. Pandey, *Advances in Chemical Pollution, Environmental Management and Protection*, Elsevier, 2021, vol. 7, pp. 65–91.
5 E. David and V.-C. Niculescu, Volatile Organic Compounds (VOCs) as Environmental Pollutants: Occurrence and Mitigation Using Nanomaterials, *Int. J. Environ. Res. Public Health*, 2021, **18**, 13147.
6 COUNCIL DIRECTIVE 1999/13/EC, https://eur-lex.europa.eu/LexUriServ/LexUriServ.do?uri=OJ:L:1999:085:0001:0022:EN:PDF.
7 H. Furukawa, K. E. Cordova, M. O'Keeffe and O. M. Yaghi, The Chemistry and Applications of Metal-Organic Frameworks, *Science*, 2013, **341**, 974–986.
8 O. K. Farha, I. Eryazici, N. C. Jeong, B. G. Hauser, C. E. Wilmer, A. A. Sarjeant, R. Q. Snurr, S. T. Nguyen, A. Ö Yazaydın and J. T. Hupp, Metal–Organic Framework Materials with Ultrahigh Surface Areas: Is the Sky the Limit?, *J. Am. Chem. Soc.*, 2012, **134**, 15016–15021.
9 L. Song, J. Zhang, L. Sun, F. Xu, F. Li, H. Zhang, X. Si, C. Jiao, Z. Li, S. Liu, Y. Liu, H. Zhou, D. Sun, Y. Du, Z. Cao and Z. Gabelica, Mesoporous metal–organic frameworks: design and applications, *Energy Environ. Sci.*, 2012, **5**, 7508.
10 H. Deng, S. Grunder, K. E. Cordova, C. Valente, H. Furukawa, M. Hmadeh, F. Gándara, A. C. Whalley, Z. Liu, S. Asahina, H. Kazumori, M. O'Keeffe, O. Terasaki, J. F. Stoddart and O. M. Yaghi, Large-Pore Apertures in a Series of Metal-Organic Frameworks, *Science*, 2012, **336**, 1018–1023.
11 Themed issues: Metal-organic frameworks, *Chem. Soc. Rev.*, 2009, 1201; *Chem. Rev.*, 2012, 112; *Chem. Soc. Rev.*, 2014, 5415.
12 G. Sneddon, A. Greenaway and H. H. P. Yiu, The Potential Applications of Nanoporous Materials for the Adsorption, Separation, and Catalytic Conversion of Carbon Dioxide, *Adv. Energy Mater.*, 2014, **4**, 1301873.
13 H. Li, L. Li, R.-B. Lin, W. Zhou, Z. Zhang, S. Xiang and B. Chen, Porous metal-organic frameworks for gas storage and separation: Status and challenges, *EnergyChem*, 2019, **1**, 100006.
14 K. Sumida, D. L. Rogow, J. A. Mason, T. M. McDonald, E. D. Bloch, Z. R. Herm, T.-H. Bae and J. R. Long, Carbon Dioxide Capture in Metal–Organic Frameworks, *Chem. Rev.*, 2012, **112**, 724–781.
15 D.-X. Xue, Q. Wang and J. Bai, Amide-functionalized metal–organic frameworks: Syntheses, structures and improved gas storage and separation properties, *Coord. Chem. Rev.*, 2019, **378**, 2–16.
16 B. Thitakamol, A. Veawab and A. Aroonwilas, Environmental impacts of absorption-based CO2 capture unit for post-combustion treatment of flue gas from coal-fired power plant, *Int. J. Greenhouse Gas Control*, 2007, **1**, 318–342.
17 P. Hajivand, J. Carolus Jansen, E. Pardo, D. Armentano, T. F. Mastropietro and A. Azadmehr, Application of metal-organic frameworks for sensing of VOCs and other volatile biomarkers, *Coord. Chem. Rev.*, 2024, **501**, 215558.

18 J. Lei, R. Qian, P. Ling, L. Cui and H. Ju, Design and sensing applications of metal–organic framework composites, *TrAC, Trends Anal. Chem.*, 2014, **58**, 71–78.
19 P. Salcedo-Abraira, R. Serrano-Nieto, C. Biglione, M. Cabrero-Antonino, S. M. F. Vilela, A. A. Babaryk, D. Tilve-Martínez, A. Rodriguez-Diéguez, S. Navalón, H. García and P. Horcajada, Two Cu-Based Phosphonate Metal–Organic Frameworks as Efficient Water-Splitting Photocatalysts, *Chem. Mater.*, 2023, **35**, 4211–4219.
20 U. Nwosu and S. Siahrostami, Copper-based metal–organic frameworks for CO 2 reduction: selectivity trends, design paradigms, and perspectives, *Catal. Sci. Technol.*, 2023, **13**, 3740–3761.
21 M. A. Halcrow, Jahn–Teller distortions in transition metal compounds, and their importance in functional molecular and inorganic materials, *Chem. Soc. Rev.*, 2013, **42**, 1784–1795.
22 J. M. Seco, D. Fairen-Jimenez, A. J. Calahorro, L. Méndez-Liñán, M. Pérez-Mendoza, N. Casati, E. Colacio and A. Rodríguez-Diéguez, Modular structure of a robust microporous MOF based on Cu2 paddle-wheels with high CO2 selectivity, *Chem. Commun.*, 2013, **49**, 11329.
23 C. Zhang, X. Xue, J. Liu, J. Lin, X. Zhang, J. Kasemchainan, H. Gao, G. Wang and X. Shu, Coordination environment dependent stability of Cu-based MOFs towards selective adsorption desulfurization, *Chem. Eng. J.*, 2023, **464**, 142670.
24 A. Karmakar, A. A. C. D. Santos, N. Pagliaricci, J. Pires, M. Batista, E. C. B. A. Alegria, A. Martin-Calvo, J. J. Gutiérrez-Sevillano, S. Calero, M. F. C. Guedes da Silva, R. Pettinari and A. J. L. Pombeiro, Halogen-Decorated Metal–Organic Frameworks for Efficient and Selective CO 2 Capture, Separation, and Chemical Fixation with Epoxides under Mild Conditions, *ACS Appl. Mater. Interfaces*, 2024, **16**(16), 20626–20641.
25 Y. An, X. Lv, W. Jiang, L. Wang, Y. Shi, X. Hang and H. Pang, The stability of MOFs in aqueous solutions—research progress and prospects, *Green Chem. Eng.*, 2024, **5**, 187–204.
26 P. N. K. De Silva, P. G. Ranjith and S. K. Choi, A study of methodologies for CO2 storage capacity estimation of coal, *Fuel*, 2012, **91**, 1–15.
27 Z. Li, P. Liu, C. Ou and X. Dong, Porous Metal–Organic Frameworks for Carbon Dioxide Adsorption and Separation at Low Pressure, *ACS Sustainable Chem. Eng.*, 2020, **8**, 15378–15404.
28 C. M. McGuirk, R. L. Siegelman, W. S. Drisdell, T. Runčevski, P. J. Milner, J. Oktawiec, L. F. Wan, G. M. Su, H. Z. H. Jiang, D. A. Reed, M. I. Gonzalez, D. Prendergast and J. R. Long, Cooperative adsorption of carbon disulfide in diamine-appended metal–organic frameworks, *Nat. Commun.*, 2018, **9**, 5133.
29 M. M. Deshmukh, M. Ohba, S. Kitagawa and S. Sakaki, Absorption of CO 2 and CS 2 into the Hofmann-Type Porous Coordination Polymer: Electrostatic versus Dispersion Interactions, *J. Am. Chem. Soc.*, 2013, **135**, 4840–4849.
30 G. M. Sheldrick, SHELXT – Integrated space-group and crystal-structure determination, *Acta Crystallogr., Sect. A: Found. Adv.*, 2015, **71**, 3–8.
31 G. M. Sheldrick, Crystal structure refinement with SHELXL, *Acta Crystallogr., Sect. C:Struct. Chem.*, 2015, **71**, 3–8.
32 O. V. Dolomanov, L. J. Bourhis, R. J. Gildea, J. A. K. Howard and H. Puschmann, OLEX2 : a complete structure solution, refinement and analysis program, *J. Appl. Crystallogr.*, 2009, **42**, 339–341.
33 (*a*) CCDC 2402172: Experimental Crystal Structure Determination, 2025, DOI: **10.5517/ccdc.csd.cc2lmnfb**; (*b*) CCDC 2402173: Experimental Crystal Structure Determination, 2025, DOI: **10.5517/ccdc.csd.cc2lmngc**; (*c*) CCDC 2402174: Experimental Crystal Structure Determination, 2025, DOI: **10.5517/ccdc.csd.cc2lmnhd**; (*d*) CCDC 2402175: Experimental Crystal Structure Determination, 2025, DOI: **10.5517/ccdc.csd.cc2lmnjf**; (*e*) CCDC 2402176: Experimental Crystal Structure Determination, 2025, DOI: **10.5517/ccdc.csd.cc2lmnkg**; (*f*) CCDC 2402177: Experimental Crystal Structure Determination, 2025, DOI: **10.5517/ccdc.csd.cc2lmnlh**; (*g*) CCDC 2402178: Experimental Crystal Structure Determination, 2025, DOI: **10.5517/ccdc.csd.cc2lmnmj**.